Two-Dimensional Compressed Correlator for Fast Acquisition of BOC(m, n) Signals

Binhee Kim, *Student Member, IEEE*, and Seung-Hyun Kong, *Member, IEEE*

Abstract—The long spreading code and the binary offset carrier (BOC) modulation technique are used in the next-generation Global Navigation Satellite System (GNSS) to improve positioning performance and to reduce inter-GNSS interference; however, the signal acquisition process of a GNSS receiver can take more time and requires additional hardware resources than legacy Global Positioning System (GPS) receivers. This paper presents the BOC 2-D compressed correlator (TDCC) technique for the fast acquisition of the next-generation GNSS signals. In the proposed BOC-TDCC, signal power in neighboring code-phase hypotheses and Doppler frequency hypotheses can be coherently combined and tested by a single compressed correlator in the first stage, and the conventional correlator-based serial search technique is employed in the second stage to test each hypothesis combined in the first stage. The performance of the BOC-TDCC is demonstrated with numerous Monte Carlo simulations and tested with real data. The BOC-TDCC has much lower mean acquisition time (MAT) than other conventional search schemes, which demonstrates that the BOC-TDCC is an effective search scheme for next-generation GNSS signals.

Index Terms—Acquisition, binary offset carrier (BOC), compressed correlator, double-dwell search.

I. INTRODUCTION

TO MEET the increasing demand for improved positioning performance and ubiquitous availability of Global Navigation Satellite System (GNSS), the next-generation GNSS has been planned and is being deployed [1]–[4]. The U.S. government announced the Global Positioning System (GPS) modernization initiative that called for the addition of two new civil signals and one new military signal to GPS satellites [2]. The European Union decided to pursue Galileo, their own GNSS, which was specifically designed for worldwide civilian use in 1998 [2]. In addition, the Global Navigation Satellite System of Russia is planning to have a new civil signal, and the Chinese Compass system is expected to be globally available in the near future [2].

The next-generation GNSS employs a number of advanced features in the physical layer for performance enhancements and coexistence with the legacy GPS [2]. Some of the new features can impact on the signal acquisition performance of receivers. A longer pseudonoise (PN) code at a higher chip rate than the legacy GPS coarse acquisition (C/A) code can be an example. It is useful to improve the signal sensitivity of a GNSS receiver; however, the longer PN code has the higher number of code-phase hypotheses to search. Therefore, the signal acquisition process needs to have more hardware resources or computational capacity. Binary offset carrier (BOC) modulation employed in the Galileo satellite navigation system that reduces inter-GNSS interference has multiple peaks in the autocorrelation function (ACF), for which a receiver should have a higher search resolution, and the acquisition process has increased complexity [5].

A good number of studies for fast PN code acquisition have been introduced in the literature [6]–[22]. Fast acquisition of the long PN code in next-generation GNSS can be achieved using parallel correlators; however, the number of parallel correlators should be multiple times larger than the legacy GPS C/A code. The fast Fourier transform (FFT)-based technique is another solution, but to deal with the longer PN code, the receiver should be equipped with a digital signal processor [19] for increased size FFT and inverse FFT. The folding technique [20] and the dual folding technique [21] are some of the recent FFT-based techniques for the fast acquisition of the long PN code. In the (dual) folding technique, the correlation is performed between the folded receiver generated code signal and the (folded) incoming signal. As the number of folding increases, this technique reduces the mean acquisition time (MAT), but it suffers from signal-to-noise ratio (SNR) degradation at the same time. In addition, the deterministic compressed acquisition (DCA) technique [22] shows a fast acquisition of the long PN code with a reduced number of parallel correlators while SNR degradation is small, and the concept of the 2-D compressed correlator (TDCC) technique for the fast acquisition of simple binary phase-shift keying (BPSK) signals (i.e., BPSK-modulated PN code signals) is introduced in [23].

The BOC modulations used in GNSS are BOC(1,1) for Galileo E1, Compass B1-C$_D$ and B1-C$_P$; BOC(6,1) for Galileo E1, Compass B1-C$_D$ and B1-C$_P$; BOC(10,5) for GPS M code; BOC(15,2.5) for Compass B3-A$_D$ and B3-A$_P$; and BOC(14,2) for Compass B1$_D$ and B1$_P$. It allows improved code delay tracking while offering a spectral separation from BPSK signals due to its split spectrum [5]. However, the sampling frequency for BOC signals (i.e., BOC-modulated PN code signals) should be higher than BPSK signals, and the BOC-ACF output (i.e., the

ACF output of BOC-modulated PN code signals) has a more complicated shape than that of BPSK signals. In [22], it has been shown that the DCA can be applied to the fast acquisition of long PN code signals with BOC modulation when the subcarrier rate is equal to the code chip rate. However, the DCA is not applicable to the BOC signals with a faster subcarrier rate than the code rate, requiring a faster sampling rate than twice the chip rate and a sophisticated detection strategy due to the multiple peaks in the ACF output. The TDCC technique introduced in [23] achieves fast acquisition of BPSK signals, but it is not suitable for BOC signals.

Techniques for the fast acquisition of BOC signals have been rarely studied. In this paper, we propose the BOC-TDCC for the fast acquisition of long PN code signals with various BOC modulations. The BOC-TDCC obtains rough estimates of the PN code phase and Doppler frequency of the incoming signal in the first stage using a compressed correlator and performs a fine search in the second stage with a conventional correlator. It is demonstrated that the BOC-TDCC has much lower MAT than the conventional double-dwell search technique, where the first dwell search uses a correlator with a shorter correlation length than the second dwell search. The rest of this paper is organized as follows. Section II derives mathematical analysis of the 2-D BOC-ACF output and Section III introduces the concept and algebraic analysis of the BOC-TDCC. Statistical performance analysis of the BOC-TDCC is provided in Section IV and the performance of the BOC-TDCC technique is demonstrated with Monte Carlo simulations and real data simulations in Section V. Performance comparison to other techniques is provided and discussed in Section VI, and finally, the conclusion is in Section VII.

II. TWO-DIMENSIONAL SEARCH OF THE BINARY OFFSET CARRIER SIGNAL

Let $r(t)$ denote a received and RF-to-IF downconverted BOC signal in a GNSS receiver, i.e.,

$$r(t) = \alpha D(t - \tau)P(t - \tau)sc(t - \tau)$$
$$\times \cos\left(2\pi(f_{IF} + f_D)t + \theta\right) + w(t) \quad (1)$$

where α, $D(t)$, $P(t)$, τ, f_{IF}, f_D, and θ represent the amplitude, the data at R_b bits per second, the PN code at code frequency $f_c (= 1/T_c)$ Hz, the code phase, the IF frequency, the Doppler frequency, and the unknown carrier phase, respectively. $w(t)$ represents the complex additive white Gaussian noise (AWGN) with two-sided power spectral density $N_0/2$, and the mathematical representation of the subcarrier function $sc(t)$ is represented as

$$sc(t) = \begin{cases} \text{sgn}\left(\sin(2\pi f_{sc}t)\right), & \text{for sinBOC} \\ \text{sgn}\left(\cos(2\pi f_{sc}t)\right), & \text{for cosBOC} \end{cases} \quad (2)$$

where f_{sc} is a subcarrier frequency. The BOC modulation in GNSS is a subcarrier modulation, where a direct-sequence spread-spectrum signal using a PN code $P(t)$ is multiplied by a subcarrier signal $sc(t)$ of frequency f_{sc} equal or higher than the
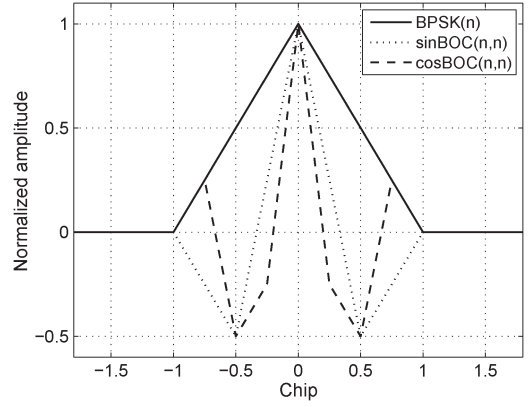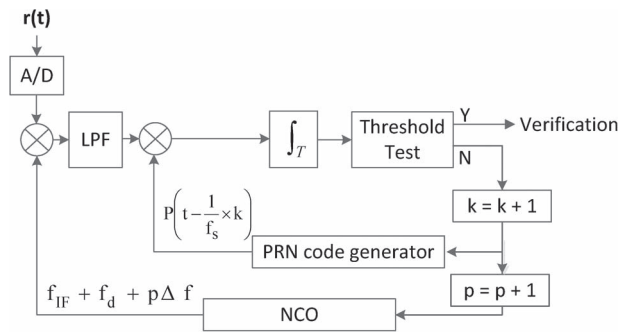

Fig. 1. Normalized 1-D ACF output.

Fig. 2. Conventional 2-D acquisition with a serial correlator.

chip rate f_c of the PN code. Denoting f_{ref} as the chip rate of the GPS C/A code at $L1$ frequency, a BOC modulation is generally represented by BOC(m, n), where $m = f_{sc}/f_{ref}$, $n = f_c/f_{ref}$, and m and n are constrained to be positive integers, and the ratio $2m/n$ is a positive integer [5]. To search the received BOC signal $r(t)$, the GNSS receiver generates a BOC signal $r_0(t)$ as

$$r_0(t) = P(t - \tau_l)sc(t - \tau_l)e^{j2\pi(f_{IF} + f_d + p\Delta f)t} \quad (3)$$

where τ_l represents the code phase of the current code-phase hypothesis (lth code-phase hypothesis) being tested by the receiver, f_d represents the Doppler frequency of the smallest Doppler frequency hypothesis made by the receiver, Δf represents the frequency search step size, and p represents the index of the current Doppler frequency hypothesis. When $|\tau_l - \tau|$ is small and $f_D = f_d + p\Delta f$, the correlation between $r(t)$ (1) and $r_0(t)$ (3) yields an ACF output shown in Fig. 1, which includes the normalized 1-D ACF output of BPSK(n), cosBOC(n, n), and sinBOC(n, n). As shown, the BOC-ACF output, i.e., the ACF output of the BOC signal, has multiple peaks within $[-1, 1]$ chips of the true PN code phase, whereas the BPSK-ACF output has a single peak and an equilateral triangular shape. The sign of the peaks in the BOC-ACF output changes with a period of $1/f_{sc}$.

In practice, the GNSS signal search is a 2-D hypothesis testing, i.e., correlating an incoming signal with a receiver generated signal made with a code-phase hypothesis and a Doppler frequency hypothesis. Fig. 2 shows the conventional

2-D acquisition process with a serial correlator, which generates an BOC-ACF output as

$$
\begin{aligned}
R(\delta\tau_l, \delta f_p) \\
= \frac{1}{T} \int_{t}^{t+T} r(u)r_0^*(u)du \Big|_{t=t_0} \\
= \frac{\alpha D}{T} \int_{t_0}^{t_0+T} P(u)sc(u)P(u-\delta\tau)sc(u-\delta\tau)e^{j(2\pi\delta f_p u+\theta)} \\
+ n(t)P(u-\tau_l)sc(u-\tau_l)e^{-j(2\pi(f_{IF}+f_d+p\Delta f)u)}du \quad (4)
\end{aligned}
$$

where t_0 is the time when the correlation (4) starts, $\delta\tau_l = \tau - \tau_l$, $\delta f_p = f_D - (f_d + p\Delta f)$, and T is the correlation length. In the following analysis, we neglect the effect of data transition and the second integrand of (4), and for algebraic simplicity, we assume $\alpha = D(t) = 1$. The mathematical expression for $R(\delta\tau_l, \delta f_p)$ of $\text{sinBOC}(n,n)$ can be derived in two separate regions, namely, $|\delta\tau_l| < T_c/2$ and $|\delta\tau_l| >= T_c/2$, such that

$$
\sum_{d=0}^{\frac{T}{T_c}-1} \frac{1}{T} \left[\int_{t_0+T_cd}^{t_0+T_cd+|\delta\tau_l|} P(u)P(u-\delta\tau_l)e^{j(2\pi\delta f_p u+\theta)}du \right.
$$

$$
+ \int_{t_0+T_cd+|\delta\tau_l|}^{t_0+T_cd+\frac{T_c}{2}} e^{j(2\pi\delta f_p u+\theta)}du
$$

$$
+ \int_{t_0+T_cd+\frac{T_c}{2}}^{t_0+T_cd+|\delta\tau_l|+\frac{T_c}{2}} -e^{j(2\pi\delta f_p u+\theta)}du
$$

$$
+ \left. \int_{t_0+T_cd+|\delta\tau_l|+\frac{T_c}{2}}^{t_0+T_c(d+1)} e^{j(2\pi\delta f_p u+\theta)}du \right]
$$

$$
\simeq \sum_{d=0}^{\frac{T}{T_c}-1} \frac{1}{j2\pi\delta f_p T} e^{j(2\pi\delta f_p(t_0+T_cd)+\theta)}
$$

$$
\times \left[e^{j\left(2\pi\delta f_p \frac{T_c}{2}\right)} - e^{j(2\pi\delta f_p|\delta\tau_l|)} - e^{j\left(2\pi\delta f_p\left(|\delta\tau_l|+\frac{T_c}{2}\right)\right)} \right.
$$

$$
\left. + e^{j\left(2\pi\delta f_p \frac{T_c}{2}\right)} + e^{j(2\pi\delta f_p T_c)} - e^{j\left(2\pi\delta f_p\left(|\delta\tau_l|+\frac{T_c}{2}\right)\right)} \right]
$$

$$
= \frac{1}{j2\pi\delta f_p T} \cdot \frac{1-e^{j2\pi\delta f_p T}}{1-e^{j2\pi\delta f_p T_c}} \cdot e^{j(2\pi\delta f_p t_0+\theta)}
$$

$$
\times \left[e^{j\left(2\pi\delta f_p \frac{T_c}{2}\right)} - e^{j(2\pi\delta f_p|\delta\tau_l|)} - e^{j\left(2\pi\delta f_p\left(|\delta\tau_l|+\frac{T_c}{2}\right)\right)} \right.
$$

$$
\left. + e^{j\left(2\pi\delta f_p \frac{T_c}{2}\right)} + e^{j(2\pi\delta f_p T_c)} - e^{j\left(2\pi\delta f_p\left(|\delta\tau_l|+\frac{T_c}{2}\right)\right)} \right]
$$

$$
= \text{sinc}(\pi\delta f_p T) \cdot \left[\frac{\sin(\pi\delta f_p(T_c/2 - |\delta\tau_l|))}{\sin(\pi\delta f_p T_c/2)} \right.
$$

$$
\left. - \frac{\sin(\pi\delta f_p|\delta\tau_l|)}{\sin(\pi\delta f_p T_c)} \right]
$$

$$
\cdot e^{j\left(2\pi\delta f_p\left(t_0+\frac{T}{2}+\frac{|\delta\tau_l|}{2}\right)+\theta\right)} \quad (5)
$$

for $|\delta\tau_l| < T_c/2$, and

$$
\sum_{d=0}^{\frac{T}{T_c}-1} \frac{1}{T} \left[\int_{t_0+T_cd}^{t_0+T_cd+|\delta\tau_l|} P(u)P(u-\delta\tau_l)e^{j(2\pi\delta f_p u+\theta)}du \right.
$$

$$
+ \left. \int_{t_0+T_cd+|\delta\tau_l|}^{t_0+T_c(d+1)} -e^{j(2\pi\delta f_p u+\theta)}du \right]
$$

$$
\simeq \text{sinc}(\pi\delta f_p T) \cdot \frac{\sin(\pi\delta f_p(|\delta\tau_l| - T_c))}{\sin(\pi\delta f_p T_c)}
$$

$$
\times e^{j\left(2\pi\delta f_p\left(t_0+\frac{T}{2}+\frac{|\delta\tau_l|}{2}\right)+\theta\right)} \quad (6)
$$

for $|\delta\tau_l| >= T_c/2$, exploiting similar algebraic manipulations used in (5). Note that the magnitude of $\text{sinBOC}(n,n)$ in (5) collapses to $\text{sinc}(\pi\delta f_p T)$ when $\delta\tau_l = 0$ and that the magnitudes of $\text{sinBOC}(n,n)$ in (5) and (6) become $(T_c - 3|\delta\tau_l|)/T_c$ and $(|\delta\tau_l| - T_c)/T_c$, respectively, when $\delta f_p = 0$. Fig. 3(a) shows a simulated 2-D $\text{sinBOC}(n,n)$ ACF output obtained from signal autocorrelation as in (4), where $\alpha = D(t) = 1$ is assumed, and the effect of $n(t)$ is neglected. As shown, the magnitude of the $\text{sinBOC}(n,n)$ ACF output has three peaks along the $\delta\tau_l$ axis due to the subcarrier, and the phase of the $\text{sinBOC}(n,n)$ ACF output changes as δf_p changes. Fig. 3(b) shows a numerical evaluation of the 2-D $\text{sinBOC}(n,n)$ ACF output expression (5) and (6) and shows a good match with the simulated 2-D $\text{sinBOC}(n,n)$ ACF output. The difference between (4), as well as (5) and (6) is numerically evaluated and shown in Fig. 3(e), where the maximum difference in magnitude and phase are 0.02 and 0.4, respectively.

The mathematical expression for $R(\delta\tau_l, \delta f_p)$ (4) of the $\text{cosBOC}(n,n)$ ACF output can be derived in four separate regions, namely $|\delta\tau_l| < T_c/4$, $T_c/4 <= |\delta\tau_l| < T_c/2$, $T_c/2 <= |\delta\tau_l| < 3T_c/4$, and $3T_c/4 < |\delta\tau_l|$, such that

$$
\sum_{d=0}^{\frac{T}{T_c}-1} \frac{1}{T} \left[\int_{t_0+T_cd}^{t_0+T_cd+|\delta\tau_l|} P(u)sc(u)P(u-\delta\tau_l)sc(u-\delta\tau_l) \right.
$$

$$
\times e^{j(2\pi\delta f_p u+\theta)}du + \int_{t_0+T_cd+|\delta\tau_l|}^{t_0+T_cd+\frac{T_c}{4}} e^{j(2\pi\delta f_p u+\theta)}du
$$

$$
+ \int_{t_0+T_cd+\frac{T_c}{4}}^{t_0+T_cd+|\delta\tau_l|+\frac{T_c}{4}} -e^{j(2\pi\delta f_p u+\theta)}du
$$

$$
+ \int_{t_0+T_cd+|\delta\tau_l|+\frac{T_c}{4}}^{t_0+T_cd+\frac{3T_c}{4}} e^{j(2\pi\delta f_p u+\theta)}du
$$

$$
+ \int_{t_0+T_cd+\frac{3T_c}{4}}^{t_0+T_cd+|\delta\tau_l|+\frac{3T_c}{4}} -e^{j(2\pi\delta f_p u+\theta)}du
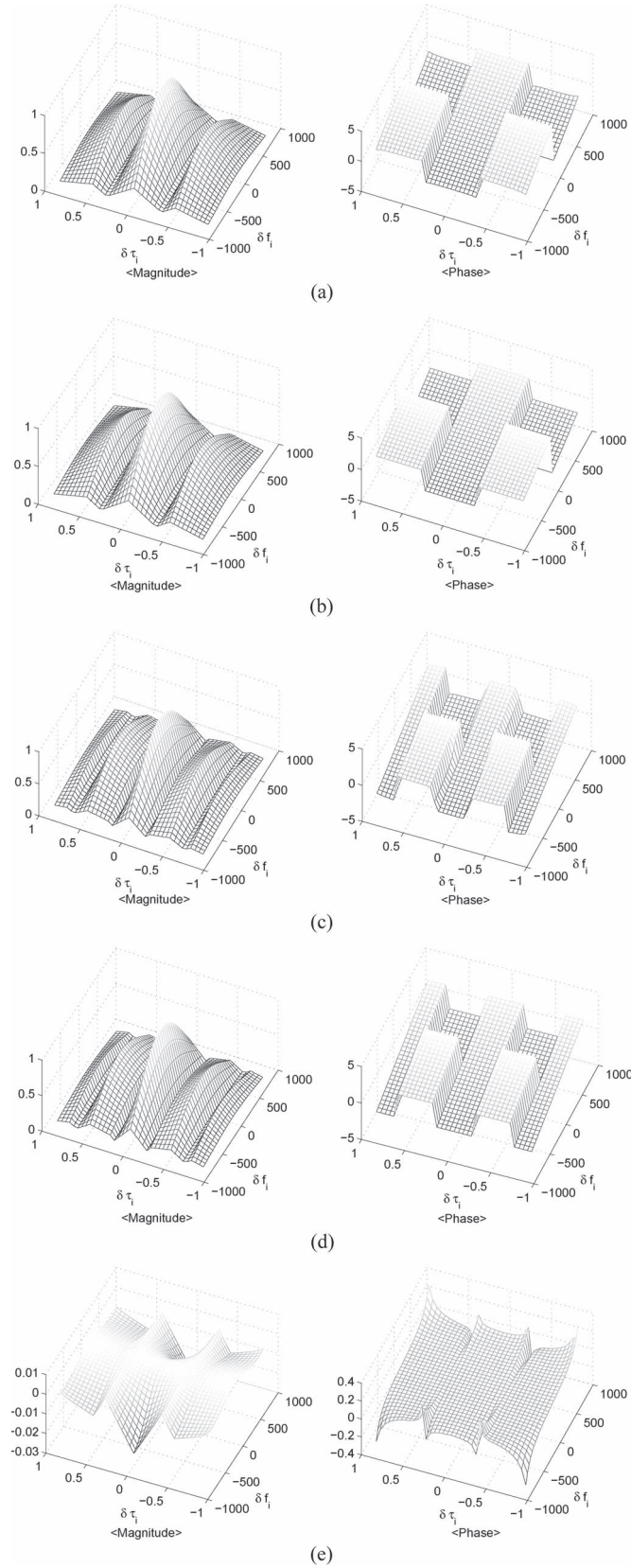$$

Fig. 3. Magnitude and phase of the 2-D ACF output. (a) Simulated 2-D sinBOC(n, n) ACF output using (4). (b) Modeled 2-D sinBOC(n, n) ACF output in (5) and (6). (c) Simulated 2-D cosBOC(n, n) ACF output using (4). (d) Modeled 2-D cosBOC(n, n) ACF output in (7)–(10). (e) Difference between (4)–(6).

$$
+ \int_{t_0+T_c d+|\delta\tau_l|+\frac{3T_c}{4}}^{t_0+T_c(d+1)} e^{j(2\pi\delta f_p u+\theta)} du \Bigg] \simeq \mathrm{sinc}(\pi\delta f_p T)
$$

$$
\cdot \left[\frac{\sin(\pi\delta f_p(T_c-|\delta\tau_l|))}{\sin(\pi\delta f_p T_c)} \right.
$$

$$
\left. - \frac{2\left(\sin\left(\pi\delta f_p\left(\frac{T_c}{2}+|\delta\tau_l|\right)\right)-\sin\left(\pi\delta f_p\left(\frac{T_c}{2}-|\delta\tau_l|\right)\right)\right)}{\sin(\pi\delta f_p T_c)} \right]
$$

$$
\times e^{j\left(2\pi\delta f_p\left(t_0+\frac{T}{2}+\frac{|\delta\tau_l|}{2}\right)+\theta\right)} \tag{7}
$$

for $|\delta\tau_l| < T_c/4$

$$
\sum_{d=0}^{\frac{T}{T_c}-1} \frac{1}{T} \Bigg[\int_{t_0+T_c d}^{t_0+T_c d+|\delta\tau_l|} P(u)sc(u)P(u-\delta\tau_l)
$$

$$
\times sc(u-\delta\tau_l)e^{j(2\pi\delta f_p u+\theta)} du
$$

$$
+ \int_{t_0+T_c d+|\delta\tau_l|}^{t_0+T_c d+\frac{T_c}{4}+|\delta\tau_l|} -e^{j(2\pi\delta f_p u+\theta)} du
$$

$$
+ \int_{t_0+T_c d+\frac{T_c}{4}+|\delta\tau_l|}^{t_0+T_c d+\frac{3T_c}{4}} -e^{j(2\pi\delta f_p u+\theta)} du
$$

$$
+ \int_{t_0+T_c d+\frac{3T_c}{4}}^{t_0+T_c(d+1)} e^{j(2\pi\delta f_p u+\theta)} du \Bigg]
$$

$$
\simeq \mathrm{sinc}(\pi\delta f_p T) \cdot \left[\frac{\sin(\pi\delta f_p(|\delta\tau_l|-T_c))}{\sin(\pi\delta f_p T_c)} \right.
$$

$$
\left. - \frac{2\sin\left(\pi\delta f_p\left(|\delta\tau_l|-\frac{T_c}{2}\right)\right)}{\sin(\pi\delta f_p T_c)} \right]
$$

$$
\cdot e^{j\left(2\pi\delta f_p\left(t_0+\frac{T}{2}+\frac{|\delta\tau_l|}{2}\right)+\theta\right)} \tag{8}
$$

for $T_c/4 <= |\delta\tau_l| < T_c/2$

$$
\sum_{d=0}^{\frac{T}{T_c}-1} \frac{1}{T} \Bigg[\int_{t_0+T_c d}^{t_0+T_c d+|\delta\tau_l|} P(u)sc(u)P(u-\delta\tau_l)sc(u-\delta\tau_l)
$$

$$
\times e^{j(2\pi\delta f_p u+\theta)} du + \int_{t_0+T_c d+|\delta\tau_l|}^{t_0+T_c d+\frac{3T_c}{4}} -e^{j(2\pi\delta f_p u+\theta)} du
$$

$$
+ \int_{t_0+T_c d+\frac{3T_c}{4}}^{t_0+T_c(d+1)} e^{j(2\pi\delta f_p u+\theta)} du \Bigg]
$$

$$
\simeq \mathrm{sinc}(\pi\delta f_p T) \cdot \left[\frac{\sin(\pi\delta f_p(|\delta\tau_l|-T_c))}{\sin(\pi\delta f_p T_c)} \right.
$$

$$
\left. + \frac{2\sin\left(\pi\delta f_p\left(|\delta\tau_l|-\frac{T_c}{2}\right)\right)}{\sin(\pi\delta f_p T_c)} \right]
$$

$$
\cdot e^{j\left(2\pi\delta f_p\left(t_0+\frac{T}{2}+\frac{|\delta\tau_l|}{2}\right)+\theta\right)} \tag{9}
$$

for $T_c/2 <= |\delta\tau_l| < 3T_c/4$, and

$$\sum_{d=0}^{\frac{T}{T_c}-1} \frac{1}{T} \left[\int_{t_0+T_cd}^{t_0+T_cd+|\delta\tau_l|} P(u)sc(u)P(u-\delta\tau_l)sc(u-\delta\tau_l) \right.$$

$$\left. \times e^{j(2\pi\delta f_p u+\theta)}du + \int_{t_0+T_cd+|\delta\tau_l|}^{t_0+T_c(d+1)} e^{j(2\pi\delta f_p u+\theta)}du \right]$$

$$\simeq \text{sinc}(\pi\delta f_p T) \cdot \frac{\sin(\pi\delta f_p(T_c-|\delta\tau_l|))}{\sin(\pi\delta f_p T_c)}$$

$$\times e^{j\left(2\pi\delta f_p\left(t_0+\frac{T}{2}+\frac{|\delta\tau_l|}{2}\right)+\theta\right)} \quad (10)$$

for $3T_c/4 < |\delta\tau_l|$, exploiting similar algebraic manipulations used in (5). Note that the magnitude of cosBOC(n,n) (7) is simplified to sinc$(\pi\delta f_p T)$ when $\delta\tau_l = 0$ and that the magnitudes of cosBOC(n,n) in (7)–(10) become $|(T_c-5|\delta\tau_l|)/T_c|$, $|\delta\tau_l|/T_c$, $|(3|\delta\tau_l|-2T_c)/T_c|$, and $|(T_c-|\delta\tau_l|)/T_c|$ for $|\delta\tau_l| < T_c/4$, $T_c/4 <= |\delta\tau_l| < T_c/2$, $T_c/2 <= |\delta\tau_l| < 3T_c/4$, and $3T_c/4 < |\delta\tau_l|$, respectively, when $\delta f_p = 0$. Fig. 3(c) shows a simulated 2-D cosBOC(n,n) ACF output obtained from the signal correlation as in (4), where $\alpha = D(t) = 1$, and $n(t)$ is neglected. As shown, the magnitude of the cosBOC(n,n) ACF output has five peaks due to the subcarrier, and the phase of the cosBOC(n,n) ACF output changes as δf_p changes. Fig. 3(d) shows a numerical evaluation of the 2-D cosBOC(n,n) ACF output expression in (7)–(10) and shows a good match with the simulated 2-D cosBOC(n,n) ACF output. Due to the similar tendency to the result in Fig. 3(e), the difference between (4) and (7)–(10) is not shown in this paper.

III. BINARY OFFSET CARRIER TWO-DIMENSIONAL COMPRESSED CORRELATOR

From the plots of the BOC-ACF output in Fig. 3, we can deduce that the test yields a useful amount of signal energy when the tested code-phase and Doppler frequency hypotheses are close to those of the incoming signal. The key idea behind the BOC-TDCC is that the signal energy found in all neighboring hypotheses can be coherently combined so that the SNR loss in the BOC-ACF output can be minimum. The BOC-ACF output has sign changes at f_{sc} hertz, and the sign change should be considered appropriately when combining the neighboring code-phase hypotheses. Fig. 4 shows an illustration of combining neighboring code-phase hypotheses into a compressed hypothesis. As shown, a compressed code-phase hypothesis is made from individual code-phase hypotheses at $1/f_{sc}$ apart and coherently combined to maximize the output signal energy. Along the axis of the Doppler frequency, the BOC-ACF output has 90° phase shift at each individual Doppler frequency hypothesis. Consider the following expression of sinBOC(n,n) ACF for $|\delta\tau_l| < T_c/2$ from (5):

$$R(0, \delta f_p + \Delta f i)$$
$$= R\left(0, \delta f_p + \frac{i}{2T}\right)$$
$$= \text{sinc}\left(\pi\left(\delta f_p + \frac{i}{2T}\right)T\right) e^{j\left(2\pi\left(\delta f_p+\frac{i}{2T}\right)\left(t_0+\frac{T}{2}\right)+\theta\right)} \quad (11)$$
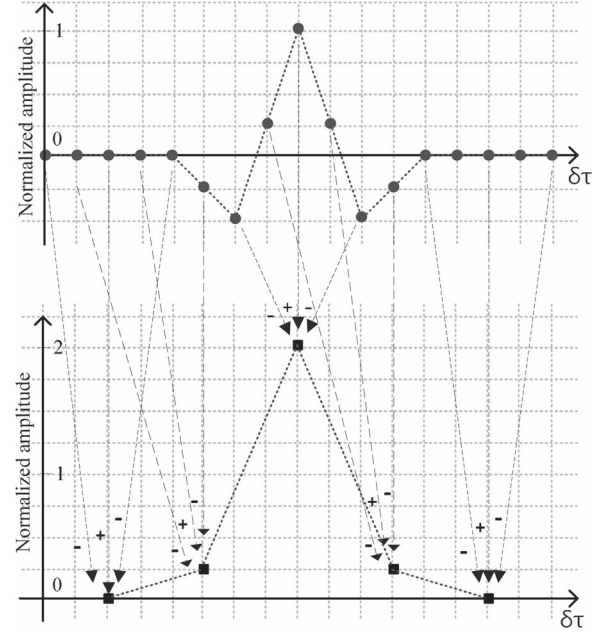

Fig. 4. Compression of the code sequence with BOC modulation ($C_c = 3$, $m = 1, n = 1$, and $f_s = 2mf_{\text{ref}}$).

where i represents the index of neighboring Doppler frequency hypotheses. From (11), the terms that dominate the phase of the sinBOC(n,n) ACF output are $e^{j(2\pi(\delta f_p+(i/2T))t_0+\theta)}$ and $e^{j\pi(\delta f_p+(i/2T))T}$. However, $e^{j(2\pi(\delta f_p+(i/2T))t_0)}$ can be negligible since a receiver can set $t_0 = 0$ when it starts to generate an IF signal with a given Doppler frequency. The only factor left is $e^{j(\pi(\delta f_p+(i/2T))T+\theta)}$ that contributes 90° phase shift between the neighboring individual Doppler frequency hypothesis. The dominating phase components and their effects are the same for other cases, including sinBOC(n,n) ACF for $|\delta\tau_l| >= T_c/2$ in (6) and sinBOC(n,n) in (7)–(10). Therefore, a 90° phase shift should be adequately compensated to coherently combine signal energy in the neighboring Doppler frequency hypotheses.

The receiver builds a compressed correlator that utilizes a compressed code-phase signal and a compressed Doppler frequency signal to coherently combine the signal energy in neighboring code-phase hypotheses and neighboring Doppler frequency hypotheses. The compressed Doppler frequency signal is a coherent sum of C_f Doppler frequency signals as

$$f_0(t, p) = \sum_{p_s=0}^{C_f-1} e^{\left(j2\pi(f_{\text{IF}}+f_d+p_s\Delta f+p\Delta fC_f)t-j\frac{p_s\pi}{2}\right)} \quad (12)$$

and the compressed code-phase signal is a coherent sum of C_c PN code sequences with the BOC modulation as

$$c_0(t, l) = \sum_{l_s=0}^{C_c-1} (-1)^{l_s} \times P\left(t - \left\lfloor \frac{l}{f_s/f_{\text{sc}}} \right\rfloor \times \frac{C_c}{f_{\text{sc}}}\right.$$
$$\left. - \text{mod}\left(l, \frac{f_s}{f_{\text{sc}}}\right) \times \frac{1}{f_s} - \frac{1}{f_{\text{sc}}} \times l_s\right). \quad (13)$$

The proposed BOC-TDCC is shown in Fig. 5. The receiver generated compressed signals $f_0(t, p)$ and $c_0(t, l)$ are multiplied
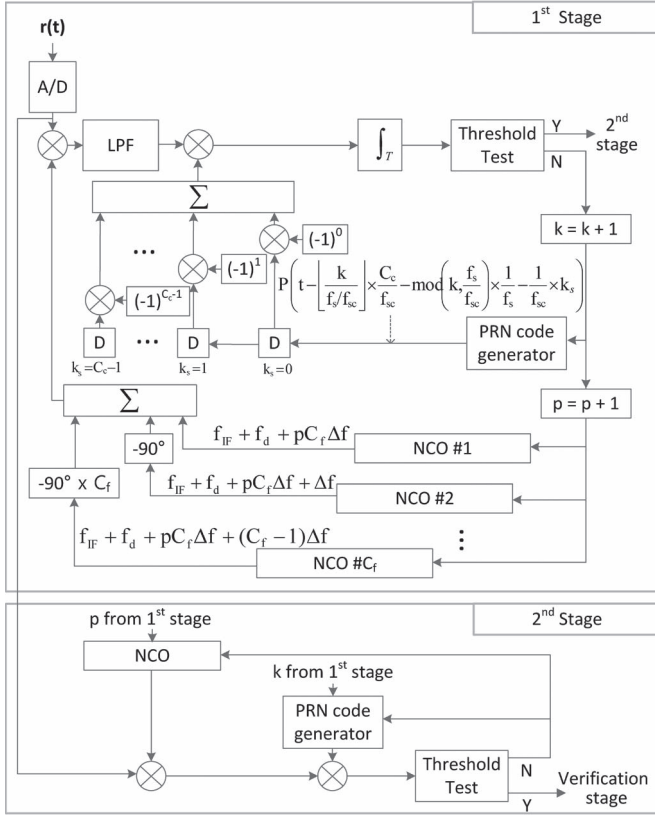
Fig. 5. Proposed 2-D compressed acquisition with a serial correlator.

to the incoming signal $r(t)$ and then integrated and squared to yield a decision variable

$$Z^1 = \left(Z_I^1\right)^2 + \left(Z_Q^1\right)^2 \tag{14}$$

of the first stage, where $Z_I^1 + jZ_Q^1$ is expressed as

$$Z_I^1 + jZ_Q^1 = \sum_{\{l,p\}} R(\delta\tau_l, \delta f_p) = \frac{1}{T}\int_0^T r(t)f_0^*(t)c_0(t)\,dt. \tag{15}$$

The decision variable Z^1 is then compared with the first stage detection threshold γ_1. When $Z^1 > \gamma_1$, all individual N_2 ($= C_c C_f$) hypotheses that constitute the current compressed hypothesis are individually tested with a conventional correlator in the second stage. The second stage can be performed with a serial or a parallel correlator technique. The second stage decision variable Z^2 is then compared to the second stage detection threshold γ_2 to find the most correct Doppler frequency and code-phase hypothesis.

IV. PERFORMANCE ANALYSIS

In this paper, we assume that sampling frequency f_s is two times the subcarrier frequency

$$f_s = 2mf_{\text{ref}} = 2f_{\text{sc}} \tag{16}$$

to meet the resolution required for the tracking loop [5]. Since the noise in the ACF output obtained with the proposed

BOC-TDCC (i.e., the first stage output) can be expressed as

$$n^1(t) = \frac{1}{T}\int_0^T n(t)f_0^*(t)c_0(t)dt \tag{17}$$

and $n(t)$, $f_0(t)$, and $c_0(t)$ are mutually independent, the variance of $n^1(t)$ can be obtained as [22]

$$V_1 = 2\sigma_f^2\sigma_P^2 m f_{\text{ref}} T N_0 \tag{18}$$

where σ_f^2 and σ_P^2 are the variances of $f_0(t)$ and $c_0(t)$, respectively. Letting $P(T_s k) = P[k]$ and $c_0(T_s k) = c_0[k]$, the compressed code-phase signal $c_0[k]$ is expressed as

$$c_0[k] = \sum_{l=0}^{C_c-1} P[k - 2l]$$

$$= \sum_{l=0}^{C_c-1} P\left[k - \left\lfloor\frac{l+k-2}{2m}\right\rfloor \cdot 2m\right]. \tag{19}$$

The noise in the kth sample of the received signal is multiplied with $c_0[k]$ so that the noise variance is amplified by $|c_0[k]|$. In $c_0[k]$, a code value can be added multiple times due to $f_s > f_{\text{sc}}$. Therefore, denoting n_s as the number of the same codes in one compressed code sample, the noise variance due to the compressed code is increased by n_s^2 times. In addition, denoting n_d as the number of different codes in one compressed code sample, the noise variance due to the compressed code is amplified by n_d times. Since the amplification of the noise in each sample is different depending on f_s and C_c, σ_P^2 can be found as

$$\sigma_P^2 = \begin{cases} \frac{4m-1}{m}, & \text{for } C_c = 2 \\ \frac{9m-4}{m}, & \text{for } C_c = 3 \\ \frac{16m-10}{m}, & \text{for } C_c = 4. \end{cases} \tag{20}$$

Since

$$\frac{1}{T}\int_0^T |f_0(t)|^2 dt = \frac{1}{T}\int_0^T \left|\sum_{n=0}^{C_f-1} e^{j\left(\frac{t}{T}-\frac{1}{2}\right)n\pi}\right|^2 dt$$

$$= C_f + \sum_{n=1}^{\lfloor\frac{C_f}{2}\rfloor} \frac{4(-1)^{n+1}(C_f - 2n + 1)}{(2n-1)\pi}$$

$$\simeq 2C_f - 1 \tag{21}$$

the variance of $n^1(t)$ can be expressed as

$$V_1 \simeq 2(2C_f - 1)\sigma_P^2 m f_{\text{ref}} T N_0. \tag{22}$$

The ACF output amplitude observed in the correct compressed hypothesis H_1^c (i.e., obtained with the proposed BOC-TDCC) depends on the choice of code phases to be combined, where $(\cdot)^c$ denotes the compressed hypothesis. For example, in Fig. 4, the compressed hypothesis H_1^c can generate the maximum
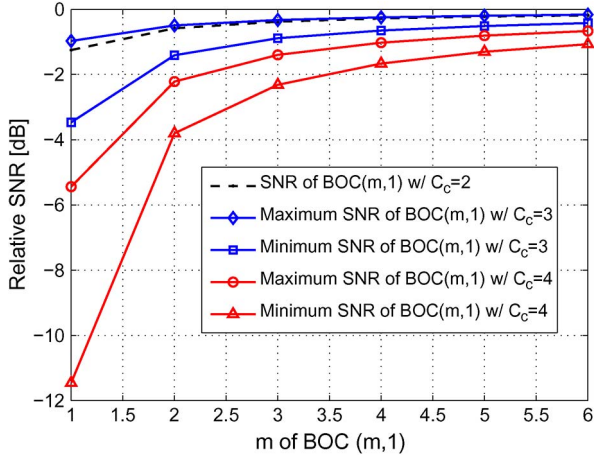
Fig. 6.   Relative SNR to BOC(1,1) with $C_f = 1$.

amplitude due to the true hypothesis located at the center of H_1^c. Otherwise, a compressed hypothesis H_1^c will result in a smaller amplitude. The maximum and minimum amplitudes from the H_1^c cell can be expressed in (23), shown at the bottom of the page. The SNR of Z^1 can be defined as

$$\text{SNR}|_{Z^1} = 20 \log_{10}\left(\frac{S_1}{\sqrt{V_1}}\right) \tag{24}$$

and Fig. 6 shows the SNR of Z^1 for various choices of C_c relative to the SNR of Z^1 for BOC(1,1) and $C_c = C_f = 1$ (i.e., no compressed hypothesis). The relative SNR can be calculated using (22) and (23), and it increases with m since the coherently combined signal energy increases with the sampling frequency f_s. However, the relative SNR decreases as C_c increases due to the faster increase of the noise variance V_1 (22). Note that the difference between the maximum S_1 and the minimum S_1 is decreasing with m and is less than 1 dB when $m \geq 6$. Let Z^2 denote the decision variable of the second stage, then the SNR of Z^2 can be found as [17]

$$\text{SNR}|_{Z^2} = 20 \log_{10}\left(\frac{S_2}{\sqrt{V_2}}\right) \tag{25}$$

where S_2 is the ACF output amplitude in the second stage, and the noise variance in the ACF output is

$$V_2 = 2m f_{\text{ref}} T N_0. \tag{26}$$

The decision variable Z^2 is then compared to the detection threshold γ_2 to find the individual hypothesis closest to the true code phase and Doppler frequency, and the code phase and Doppler frequency of the selected hypothesis is then sent to the verification process for acquisition confirmation.
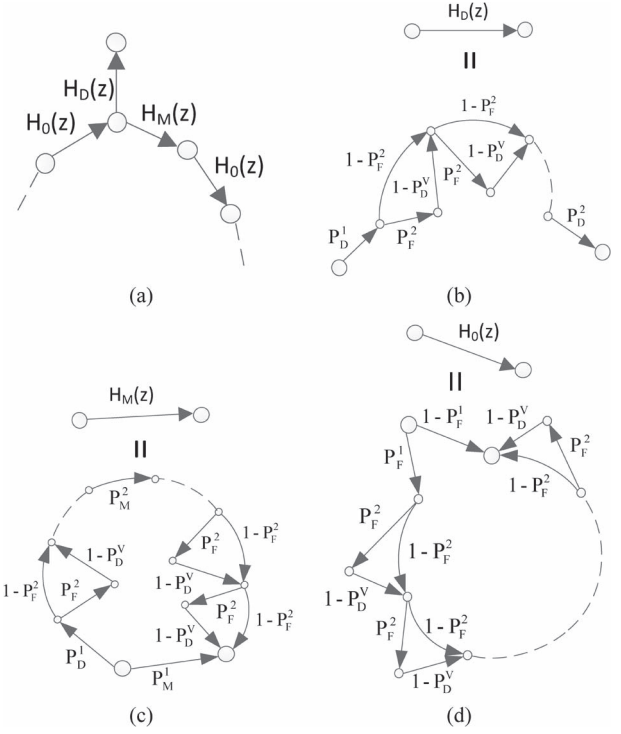

Fig. 7.   State diagram of the BOC-TDCC. (a) State diagram of TDCC. (b) $H_D(z)$. (c) $H_M(z)$. (d) $H_0(z)$

In AWGN, probabilities of detection, miss, and false alarm are found in [17] as

$$P_D^i = Q\left(S_i\sqrt{\frac{2}{V_i}}, \sqrt{\frac{2\gamma_i}{V_i}}\right) \tag{27}$$

$$P_M^i = 1 - P_D^i \tag{28}$$

$$P_F^i = \exp\left(-\frac{\gamma_i}{V_i}\right) \tag{29}$$

where $Q(a, b)$ is the Marcum's Q-function [24]. Fig. 7 shows the state diagram of the proposed BOC-TDCC. If the current compressed hypothesis H^c is the correct compressed hypothesis H_1^c (i.e., H^c includes the correct hypothesis H_1), the hypothesis testing may have a successful signal detection with probability P_D^1 or miss the signal detection with probability P_M^1. On the other hand, if the current compressed hypothesis is incorrect ($H^c = H_0^c$), it may conclude the absence of signal with probability $1 - P_F^1$ or may result in a false alarm with probability P_F^1. When a signal detection is declared in the first stage, the search algorithm proceeds to the second stage, where a conventional correlator is applied to test the individual hypotheses compressed into the hypothesis H^c. If the hypothesis

$$S_1 = \begin{cases} \displaystyle\sum_{p_s=0}^{C_f-1}\sum_{l_s=0}^{C_c-1} R\left(\frac{l_s}{f_s}, \Delta f \cdot p_s\right) e^{j p_s \pi/2}(-1)^{l_s}, & \text{minimum} \\ \displaystyle\sum_{p_s=0}^{C_f-1}\sum_{l_s=0}^{C_c-1} R\left(\frac{1}{f_s}\cdot(-1)^{l_s}\cdot\left\lfloor\frac{l_s+1}{2}\right\rfloor, \Delta f\cdot(-1)^{p_s}\cdot\left\lfloor\frac{p_s+1}{2}\right\rfloor\right)(-1)^{\lfloor\frac{l_s+1}{2}\rfloor} e^{j p_s \pi/2}, & \text{maximum} \end{cases} \tag{23}$$

H being tested in the second stage is the correct hypothesis (i.e., $H = H_1$), the second stage may have a successful signal detection with probability P_D^2 or miss the signal detection with probability P_M^2. If $H = H_0$, it may conclude the absence of signal with probability $1 - P_F^2$ or a false alarm with probability P_F^2. When a signal detection is declared or a false alarm is made in the second stage, the acquisition function needs to execute the verification process that takes T^{p_v} seconds. The overall branch transfer function for correct hypothesis detection can be represented as

$$H_D(T) = \begin{cases} \dfrac{(1-T^{N_2})T^2}{N_2(1-T)}, & \text{for high SNR} \\[2ex] \dfrac{\left(1-\left[(1-P_F^2)T+P_F^2T^{1+p_v}\right]^{N_2}\right)P_D^1 P_D^2 T^2}{N_2\left(1-\left[(1-P_F^2)T+P_F^2T^{1+p_v}\right]\right)}, & \text{otherwise.} \end{cases} \tag{30}$$

The overall branch transfer function for the correct hypothesis missed can be found as

$$H_M(T) = \begin{cases} 0, & \text{for high SNR} \\[1ex] P_M^1 T + P_D^1 P_M^2 T^2 \\ \quad \times \left[(1-P_F^2)T+P_F^2T^{1+p_v}\right]^{N_2-1}, & \text{otherwise} \end{cases} \tag{31}$$

and the overall branch transfer function for incorrect hypothesis can be expressed as

$$H_0(T) = \begin{cases} T, & \text{for high SNR} \\[1ex] (1-P_F^1)T + P_F^1 T \\ \quad \times \left[(1-P_F^2)T+P_F^2T^{1+p_v}\right]^{N_2}, & \text{otherwise.} \end{cases} \tag{32}$$

The overall transfer function of the proposed BOC-TDCC is expressed as

$$H(T) = \frac{H_D(T)\left[1 - H_0^{N_1}(T)\right]}{N_1\left[1 - H_0(T)\right]\left[1 - H_M(T)H_0^{N_1-1}(T)\right]} \tag{33}$$

where N_1 is the number of all compressed hypotheses to test in the first stage [17], [25]. In the proposed BOC-TDCC, the number of hypotheses to test in the first stage N_1 is much larger than that in the second stage N_2 (i.e., $N_1 \gg N_2$) so that the MAT can be derived as

$$\mu_T = \left. \frac{dH(T)}{dT} \right|_{T=1}$$
$$\simeq N_1 \left(N_2 P_F^1 \left(1 + p_v P_F^2 \right) + 1 \right) \left(\frac{1}{P_D^1 P_D^2} - \frac{1}{2} \right). \tag{34}$$

Moreover, an algebraic expression for the variation of acquisition time (VAT) can be obtained when the SNR is high as

$$\sigma_T^2 = \left(\frac{d^2H(T)}{dT^2} + \frac{dH(T)}{dT}\left[1 - \frac{dH(T)}{dT}\right] \right)\Bigg|_{T=1}$$
$$\sigma_T^2\big|_{\text{SNR}\uparrow} \simeq \frac{N_1^2}{3} + \left(\frac{N_2}{2} - 1 \right) N_1. \tag{35}$$
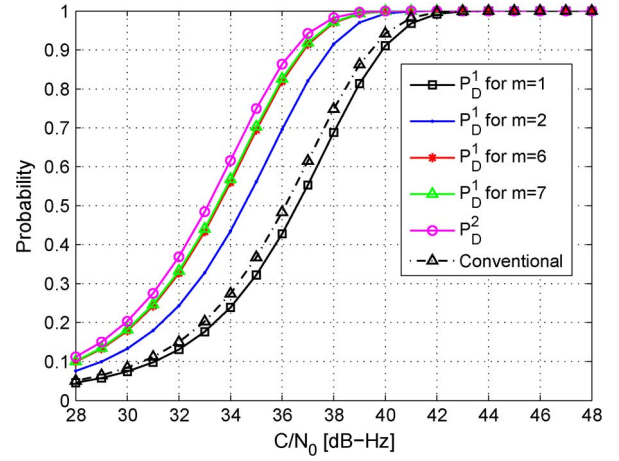

Fig. 8. Detection probability and false alarm probability ($C_c = 3$ and $C_f = 1$).

To improve the detection sensitivity of the BOC-TDCC, non-coherent accumulation of the decision variables Z^1 and Z^2 can be performed. Denoting L as the noncoherent accumulation number, detection and false alarm probabilities in AWGN can be found as [26]

$$P_D^i = Q\left(S_i \sqrt{\frac{2L}{V_i}}, \sqrt{\frac{2\gamma_i}{V_i}} \right) \tag{36}$$

$$P_F^i = \exp\left(-\frac{\gamma_i}{V_i} \right) \sum_{l=0}^{L-1} \frac{1}{l!} \left(\frac{\gamma_i}{V_i} \right)^l. \tag{37}$$

In a Rayleigh fading channel, detection and false alarm probabilities are readily available from [17] as

$$P_D^i = e^{\gamma/V_F^L} \sum_{k=0}^{L-1} \frac{(\gamma/V_F^L)^k}{k!} \tag{38}$$

$$P_F^i = \exp\left(-\frac{\gamma_i}{V_i} \right) \sum_{l=0}^{L-1} \frac{1}{l!} \left(\frac{\gamma_i}{V_i} \right)^l \tag{39}$$

where

$$V_{Fi}^L = V_i^L + S_i^2 \sigma^2 \tag{40}$$

and σ means a mode value of the Rayleigh distribution. Fig. 8 shows the detection probabilities with a fixed false alarm probability ($P_F = 10^{-2}$) of the first and second stages for various m with respect to C/N_0 (carrier-to-receiver noise density). Although BOC(1,1), BOC(10,5), BOC(6,1), BOC(15,2.5), and BOC(14,2) are used in GNSS, only the simulation results of BOC(1,1), BOC(2,1), BOC(6,1), and BOC(7,1) are provided in Fig. 8 because the SNR of the ACF output obtained with the proposed BOC-TDCC depends on the ratio m/n but does not depend on the respective values of m and n. As shown, the detection (false alarm) probability of the second stage is higher (lower) than that of the first stage. This is because of the SNR loss in the first stage for $C_c > 1$. Moreover, the detection probability increases but the false alarm probability decreases as m increases, which is due to the increased sampling frequency to handle the BOC signal with increased m. For a comparison, the
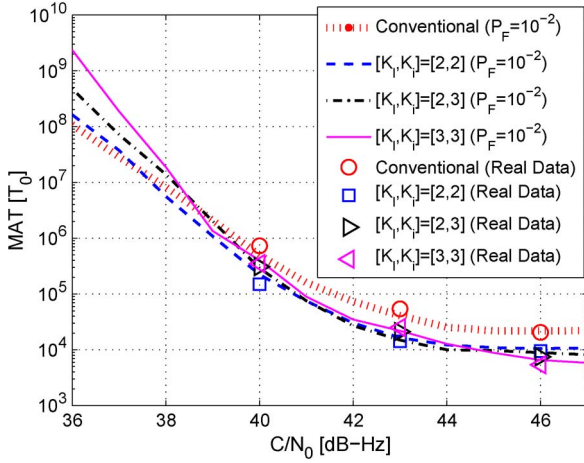
Fig. 9.   Mean acquisition time.

Fig. 10.   Variance of acquisition time.

detection probability of the conventional double-dwell search technique with the first and second stage correlation lengths 0.5 and 1 ms, respectively, is provided. As shown in Fig. 8, due to the shorter correlation length (3-dB SNR loss) in the first stage than in the second stage of the conventional double-dwell search technique, the detection probability of the conventional double-dwell search technique is lower than that of the second stage of BOC-TDCC that uses the conventional single-dwell search technique with $T = 1$ ms [17].

V. NUMERICAL RESULTS

Here, the performance of the BOC-TDCC is tested for a receiver with a bandpass filter (BPF) having 2-MHz band-width, sampling frequency $f_s = 2mf_{\text{ref}}$, correlation length $T = T_0 (= 1$ ms), and the code phase and Doppler fre-quency search step sizes equal to $1/2f_{\text{sc}}$ and $\Delta f = 500$ Hz, respectively. The PN code sequence has a chip rate $R_c = 1.023$ MHz, subcarrier frequency $f_{\text{sc}} = 1.023$ MHz, and an unknown Doppler frequency between -5 and 5 kHz. In the fol-lowing simulations, the target constant false alarm rate (P_F) is set to 10^{-2}. In practice, a BOC signal may have a chip rate that is different from 1.023 MHz; however, it is shown that the per-formance of the BOC-TDCC is only related to the ratio m/n.

Fig. 9 shows the MAT obtained from 10^4 Monte Carlo simulations for various C_c and C_f. For a comparison, the performance of the conventional double-dwell search technique with the first- and second-stage correlation lengths $0.5T_0$ and T_0, respectively, is provided. In the simulations, the proposed BOC-TDCC is used for the first stage, the conventional serial search correlator is employed for the second stage, and both stages have $T_0 = 1$ ms correlation length. As shown in the results, the proposed technique has two to five times smaller MAT than the conventional double-dwell search technique for C/N_0 higher than 40 dB Hz. Note that, for C/N_0 higher than 45 dB Hz, the MAT decreases as $C_c C_f$ increases, as expected. However, for C/N_0 lower than 40 dB Hz, larger $C_c C_f$ results in a larger MAT. This is due to the faster increase of noise variance as $C_c C_f$ increases more than the sum of the signal energy. For example, the MAT for $[C_c, C_f] = [2, 2]$ is about twice the MAT for $[C_c, C_f] = [3, 3]$ for C/N_0 higher than 45 dB Hz, because
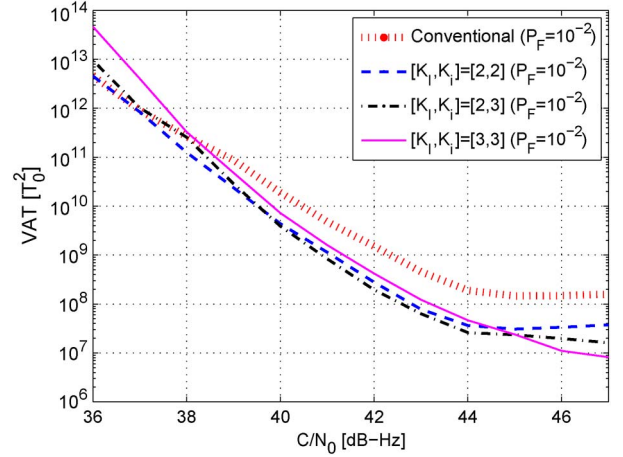
the number of compressed hypothesis for $[C_c, C_f] = [3, 3]$ is about half of $[C_c, C_f] = [2, 2]$. In fact, from (34), it is expected that the MAT can be approximated as

$$\mu_T|_{\text{SNR}\uparrow} \simeq 0.5N_1 \qquad (41)$$

when C/N_0 is large enough, which agrees with the analysis of MAT (34) and our observation in Fig. 9. Fig. 10 shows the result of 10^4 Monte Carlo simulations to evaluate the VAT of the proposed BOC-TDCC for various C_c and C_f. The conditions of the VAT simulation are the same as those of the MAT simulation. As shown, the proposed BOC-TDCC technique has more than two times smaller VAT than the conventional double-dwell search technique, and the VAT decreases as $C_c C_f$ increases for C/N_0 higher than 40 dB Hz. Moreover, for C/N_0 lower than 40 dB Hz, the simulation result shows performance degradation of the proposed BOC-TDCC technique in a similar pattern observed in the MAT simulation results, which is due to the faster increase of noise variance, as $C_c C_f$ increases, than the sum of signal energy.

To verify the simulation results, the performance of the proposed BOC-TDCC is tested with real data from a GNSS simulator. The Spirent GSS8000 GNSS simulator [27] and the Sparkfun SiGe GN3S Sampler [28] are used for GNSS simulation. Real data are sampled with 2-MHz BPF bandwidth and sampling frequency $f_s = 2mf_{\text{ref}}$, and Galileo E1 signals are collected at $C/N_0 = 40$, 43, and 46 dB Hz. The results of the real data simulation in Fig. 9 show a good match with the Monte Carlo simulation results in the same figure.

VI. COMPARISON WITH OTHER TECHNIQUES

A number of techniques in [25] and [29] use the hypothesis combining technique to reduce MAT. In [25], several tech-niques that combine multiple hypotheses for multipath are in-troduced, and in [29], it is introduced that multiple ACF outputs from neighboring code-phase hypotheses can be combined to increase the SNR and perform faster acquisition when the receiver has a higher sampling rate than the Nyquist rate (i.e., $f_s \geq 2f_c$). However, these techniques do not reduce the number of hypotheses to test; therefore, their MAT reduction is limited.

Recently, the folding technique [20], [21], [30] has been introduced for a fast acquisition of GNSS signals with long PN codes. In the folding technique, a fast acquisition can be achieved by combining multiple nonneighboring code-phase and Doppler frequency hypotheses to test; however, there is no signal power amplification from combining multiple hypotheses. On the contrary, there is some signal power amplification in the proposed BOC-TDCC since multiple neighboring hypotheses conveying some amount of signal power are coherently combined. The folding technique in [20], [21], and [30] is implemented for a parallel search scheme and uses FFT-based correlation; however, the concept of multiple hypotheses combining in the folding technique can be applied to the serial search scheme and maybe compared to the proposed BOC-TDCC. Since both the folding technique and the proposed BOC-TDCC achieves a fast acquisition by reducing the number of hypotheses to test, performance can be compared with the SNR loss for the same number of hypotheses to be combined. For example, if two code cells and two frequency cells are combined in both the folding technique and the proposed BOC-TDCC (i.e., $[C_c, C_f] = [2, 2]$), there is no signal power amplification and four times noise variance amplification in the folding technique, whereas in the proposed BOC-TDCC, the amplification of signal power and the amplification of noise variance are by $(2.25)^2$ and nine times, respectively. Therefore, the SNR loss for the folding techniques is about $10 \log 4$ dB, and the SNR loss for the proposed BOC-TDCC is about $10 \log 1.78$ dB.

In the implementation of the proposed BOC-TDCC, additional hardware is required compared with the conventional single-dwell search technique [17]. As shown in Fig. 5, multiple delay components and a summation block are required for the generation of the compressed code-phase signal $c_0[k]$. For the generation of the compressed Doppler frequency signal $f_0(t)$, the number of numerically controlled oscillators (NCO) should be C_f, and phase compensation blocks and a summation block are required. Instead of using multiple NCOs, a compressed Doppler frequency signal can be generated by using a single NCO, complex multiplications, and a summation block; since one frequency signal can be generated by the multiplication of an NCO-generated carrier signal and exponential coefficients $e^{j2\pi p_s \Delta f t}$ (12) stored in a memory, one individual frequency signal can be generated by a single NCO, and the other $C_f - 1$ carrier signals can be produced by using complex multiplications.

VII. CONCLUSION

This paper has presented the TDCC technique for the fast acquisition of BOC signals. The performance of the proposed BOC-TDCC has been analyzed, and its performance has been compared with the conventional double-dwell search technique. It has been shown that the proposed BOC-TDCC has significant advantages over the conventional double-dwell search technique, particularly when C/N_0 is high enough. The proposed TDCC has two to five times smaller MAT and two times smaller VAT than the conventional double-dwell search technique for a good C/N_0 (for example, > 40 dB). Moreover, the MAT and

VAT decrease as the total number of neighboring individual hypotheses combined into the compressed hypothesis increases when C/N_0 is high.

REFERENCES

[1] P. Misra and P. Enge, *Global Positioning System: Signals, Measurements, and Performance,* 2nd ed. Lincoln, MA, USA: Ganga-Jamuna, 2006.

[2] E. D. Kaplan and C. J. Hegarty, *Understanding GPS: Principles and Applications*, 2nd ed. Norwood, MA, USA: Artech, 2005.

[3] Galileo Open Service Signal In Space Interface Control Document. [Online]. Available: http://ec.europa.eu/enterprise/policies/satnav/index_en.htm

[4] Galileo Fact Sheet. [Online]. Available: http://www.esa.int/Our_Activities/Navigation

[5] O. Julien, C. Macabiau, M. E. Cannon, and G. Lachapelle, "ASPeCT: Unambiguous sine-BOC(n, n) acquisition/tracking technique for navigation applications," *IEEE Trans. Aerosp. Electron. Syst.*, vol. 43, no. 1, pp. 150–162, Jan. 2007.

[6] B. Parkinson, J. Spilker, P. Axelrad, and P. Enge, *Global Positioning System: Theory and Applications*. Washington, DC, USA: AIAA, 1996.

[7] P. W. Ward, "GPS Receiver Search Techniques," in *Proc. IEEE PLANS*, Atlanta, GA, USA, Apr. 1996, pp. 604–611.

[8] F. Van Diggelen, *A-GPS: Assisted GPS, GNSS, and SBAS*. Norwood, MA, USA: Artech, 2009.

[9] H. Li, M. Lu, X. Cui, and Z. Feng, "Generalized zero-padding scheme for direct GPS P-code acquisition," *IEEE Trans. Wireless Commun.*, vol. 8, no. 6, pp. 2866–2871, Jun. 2009.

[10] Y. Huang and J. Wang, "Two-stage acquisition in time-hopping impulse radio systems for UWB communications," *IEEE Trans. Wireless Commun.*, vol. 6, no. 10, pp. 3578–3588, Oct. 2007.

[11] L. Reggiani and G. M. Maggio, "Rapid search methods for code acquisition in UWB impulse radio communications," *IEEE J. Select. Areas Commun.*, vol. 23, no. 5, pp. 898–908, May 2005.

[12] S. Yeom, Y. Jung, and S. Lee, "An adaptive threshold technique for fast PN code acquisition in DS-SS systems," *IEEE Trans. Veh. Technol.*, vol. 60, no. 6, pp. 2870–2875, Jul. 2011.

[13] K. M. Chugg and M. Zhu, "A new approach to rapid PN code acquisition using iterative message passing techniques," *IEEE J. Select. Areas Commun.*, vol. 23, no. 5, pp. 884–897, May 2005.

[14] Y. H. Lee and S. Tantaratana, "Sequential acquisition of PN sequences for DS/SS communications: Design and performance," *IEEE J. Select. Areas Commun.*, vol. 10, no. 4, pp. 750–759, May 1992.

[15] Y. H. Lee and S. J. Kim, "Sequence acquisition of DS-CDMA systems employing gold sequences," *IEEE Trans. Veh. Technol.*, vol. 49, no. 6, pp. 2397–2404, Nov. 2000.

[16] J. Ibrahim and R. M. Buehrer, "Two-stage acquisition for UWB in dense multipath," *IEEE J. Select. Areas Commun.*, vol. 24, no. 4, pp. 801–807, Apr. 2006.

[17] A. J. Viterbi, *CDMA: Principles of Spread Spectrum Communication*. Reading, MA, USA: Addison-Wesley, 1995, ch. 3, pp. 39–67.

[18] E. A. Sourour and S. C. Gupta, "Direct-sequence spread-spectrum parallel acquisition in a fading mobile channel," *IEEE Trans. Commun.*, vol. 38, no. 7, pp. 992–998, Jul. 1990.

[19] D. Akopian, "Fast FFT based GPS satellite acquisition methods," *IEE Proc.-Radar Sonar Navig.*, vol. 152, no. 4, pp. 277–286, Aug. 2005.

[20] C. Yang, J. Vasquez, and J. Chaffee, "Fast direct P(Y)-code acquisition using XFAST," in *Proc. ION GPS*, Sep. 1999, pp. 317–324.

[21] H. Li, X. Cui, M. Lu, and Z. Feng, "Dual-folding based rapid search method for long PN-code acquisition," *IEEE Trans. Wireless Commun.*, vol. 7, no. 12, pp. 5286–5296, Dec. 2008.

[22] S.-H. Kong, "A deterministic compressed GNSS acquisition technique," *IEEE Trans. Veh. Technol.*, vol. 62, no. 2, pp. 511–521, Feb. 2013.

[23] B. Kim and S.-H. Kong, "Two dimensional compressed correlator for fast acquisition in GNSS," in *Proc. ION ITM*, San Diego, CA, USA, Jan. 2013, pp. 519–525.

[24] J. I. Marcum, "A Table of Q-functions," Rand Corp., Santa Monica, CA, USA, Rep. No. RM-339, Jan. 1950.

[25] M. A. Abu-Rgheff, *Introduction to CDMA Wireless Communications*. New York, NY, USA: Academic, 2007, ch. 5, pp. 253–323.

[26] C. O'Driscoll, M. G. Petovello, and G. Lachapelle, "Software receiver strategies for the acquisition and re-acquisition of weak GPS signals," in *Proc. ION ITM*, Jan. 28–30, 2008, pp. 843–854.

[27] Spirent GSS8000 Series. [Online]. Available: http://www.spirent.com/~/media/Datasheets/Positioning/GSS8000.pdf

[28] Sparkfun SiGe GN3S Sampler v3. [Online]. Available: https://www.sparkfun.com/products/10981
[29] S. Yoon, I. Song, S. Y. Kim, and S. R. Park, "A DS-CDMA code acquisition scheme robust to residual code phase offset variation," *IEEE Trans. Veh. Technol.*, vol. 49, no. 6, pp. 2405–2418, Nov. 2000.
[30] H. Li, M. Lu, and Z. Feng, "Three-stage based rapid long PN-code acquisition method by employing time–frequency folding technique," *Chin. J. Electron.*, vol. 19, no. 4, pp. 727–732, Oct. 2010.

Seung-Hyun Kong (M'06) received the B.S.E.E. degree from Sogang University, Seoul, Korea, in 1992, the M.S.E.E. degree from Polytechnic University, Brooklyn, NY, USA, in 1994, and the Ph.D. degree in aeronautics and astronautics from Stanford University, Stanford, CA, USA, in 2006.

From 1997 to 2004, he was with Samsung Electronics, Inc., and Nexpilot, Inc., both in Korea, where his research focus was on second-generation code division multiple access and third-generation universal mobile telecommunications system physical and mobile positioning technologies. In 2006, he was involved with hybrid positioning technology development using wireless location signature and assisted Global Navigation Satellite System (GNSS) with Polaris Wireless, Inc., and from 2007 to 2009, he was with the Research Staff of the Qualcomm Research Center, San Diego, CA, USA, where his R&D focus was on indoor location technologies and advanced GNSS technologies. Since 2010, he has been an Assistant Professor with the CCS Graduate School for Green Transportation, Korea Advanced Institute of Science and Technology. His research interests include superresolution signal processing, detection and estimation for navigation systems, and vehicular communication systems.

Binhee Kim (S'08) received the B.S.E.E. and M.S.E.E. degrees in 2008 and 2010, respectively, from the Korea Advanced Institute of Science and Technology, Daejeon, Korea, where she is currently working toward the Ph.D. degree with the CCS Graduate School for Green Transportation.

Her research interests include superresolution signal processing and detection and estimation for navigation systems.